JOURNAL OF AIRCRAFT
Vol. 41, No. 2, March–April 2004

Detection and Avoidance of Main Rotor Hub Moment Limits on Rotorcraft

Joseph F. Horn* and Nilesh Sahani†
Pennsylvania State University, University Park, Pennsylvania 16802

There is interest in developing carefree maneuvering capability on future rotorcraft. This has driven the need for advanced algorithms that predict the onset of structural limits and cue the pilot using tactile feedback. A new method is presented for the detection and avoidance of static load limits on the main rotor hub. An algorithm was developed that uses linear models to estimate constraints on longitudinal and lateral cyclic stick positions that ensure the transient response of hub moments remain bounded within prescribed limits. The system was tested using a high-fidelity nonlinear simulation of a UH-60A helicopter (GENHEL). The system was shown to be successful in simultaneously constraining stick travel in both lateral and longitudinal axes to prevent hub moment limit violations. The most critical conditions occurred during control reversals, at which point the system effectively imposed rate limits on the stick motion. The algorithm was shown to be robust to changes in aircraft weight and c.g. location.

Nomenclature

$\boldsymbol{A}, \boldsymbol{B}, \boldsymbol{C}$	=	state-space dynamic matrices
A_{1s}, B_{1s}	=	lateral and longitudinal cyclic pitch, deg
a_{0s}, a_{1s}, b_{1s}	=	collective, lateral and longitudinal flapping angles, rad
d	=	proximity of current stick position to the elliptical boundary, in.
d_1, d_2	=	soft stop distance parameters, in.
$\boldsymbol{E_1}, \boldsymbol{E_2}$	=	output response parameters, Eq. (8)
$\boldsymbol{F}, \boldsymbol{G}, H$	=	stick constraint parameters, Eq. (10)
$F_{\text{lat}}, F_{\text{long}}$	=	force on lateral and longitudinal stick, lb
I, K, C	=	stick inertia, spring gradient and damping coefficient, slug, lb/ft, lb · s/ft
I_y	=	helicopter pitch moment of inertia, slug · ft^2
k_{hub}	=	hub constant, ft · lb
L_H, M_H	=	lateral and longitudinal hub moment, ft · lb
M	=	total aerodynamic moment about c.g., ft · lb
$\boldsymbol{n}$	=	hub moment stick gradient vector
$\boldsymbol{P}$	=	force vector applied to cyclic stick
$\boldsymbol{P}_{\text{cue}}$	=	soft stop force vector
P_{stop}	=	magnitude of soft stop, lb
p, q, r	=	roll, pitch, and yaw rates, rad/s
t	=	time, s
$\boldsymbol{u}$	=	input vector (stick displacement)
u, v, w	=	x, y, and z components of body velocity, ft/s
V_x, V_y, V_z	=	flight-path velocities, ft/s
$\boldsymbol{x}$	=	state vector
$\boldsymbol{y}$	=	output vector (hub moments)
Δ	=	deflection from equilibrium
$\delta_{\text{lat}}, \delta_{\text{long}}$	=	lateral and longitudinal stick deflection, in.
$\zeta_0, \zeta_{1s}, \zeta_{1c}$	=	blade lag angles, rad
$\lambda_0, \lambda_{1s}, \lambda_{1c}$	=	rotor inflow ratio
φ, θ, ψ	=	roll, pitch, and yaw angles, deg

Subscripts

des	=	desired values, Eq. (16)
e	=	equilibrium value
lim	=	limiting value
pk	=	peak value
0	=	Initial condition (current value)

Superscript

$*$	=	critical value

Introduction

RECENTLY there has been increased interest in implementing carefree handling qualities on modern rotorcraft with advanced flight control systems. The terms carefree handling or carefree maneuvering refer to the capability of a pilot to fly throughout the operational flight envelope without requiring significant workload to monitor and avoid exceeding structural, aerodynamic, or control limits.[1–2] Studies have shown that handling qualities are degraded as pilots attempt to perform more aggressive maneuvers. The degradation in handling is largely due to the requirement to monitor and avoid envelope limits associated with the structural and controllability constraints on the aircraft.[1–5] Pilots must typically be conservative when maneuvering near structural limits that are not easily perceived, and as a result, the maximum agility of the aircraft is not obtained. A study conducted by Handcock et al.[5] has shown that active control technology, which encompasses fly-by-wire primary flight control, advanced control laws, and carefree handling, is fundamental to safe and effective day/night all weather operations and contributes significantly to agility, precision control, situation awareness, and crashworthiness.

A number of novel systems have been developed that predict the onset of limits and then cue the pilot of approaching limits using tactile feedback.[6–10] The tactile cueing systems impose a variable soft stop in the stick force-feel system, which allows the pilot to maneuver to the edge of the envelope without requiring excessive visual or cognitive workload to monitor limits. There are two advantages to using tactile cueing instead of limiting the aircraft response directly in the automatic flight control system (AFCS). First, whereas the pilot cannot typically override AFCS limiting, the pilot can push through a soft stop to override the limit in an emergency. Second, limiting functions in the AFCS will alter the aircraft response and result in less predictable behavior. As a result, pilots generally consider cueing systems to be a more acceptable solution.

The major technical barrier in implementing a tactile cueing system is the requirement for predictive algorithms to calculate the

Presented as Paper 2001-4138 at the AIAA Atmospheric Flight Mechanics Conference, Montreal Canada, 6 August 2001; received 2 December 2002; revision received 23 April 2003; accepted for publication 12 June 2003.

*Assistant Professor, Department of Aerospace Engineering. Member AIAA.
†Graduate Research Assistant, Department of Aerospace Engineering.

location of the soft stop. Typically, the location of the soft stop will vary as the aircraft is maneuvered and the flight condition changes. The calculation of the soft stop location must be based on the projected future response of a limited parameter. A reliable measurement of a limited parameter alone will not be sufficient due to the time lag associated with the response. It is necessary to estimate the future response of the limited parameter using a predictive algorithm such as a neural network or linear estimator. It is then necessary to invert the problem, by finding the control positions that correspond to a violation of a limit. A common approach has been to use neural networks to predict the future response of a limited parameter and then estimate the soft stop location based on the sensitivity of the parameter to the pilot control inputs.[6,9,10] The neural network prediction can then be adapted based on the measured response of the limited parameters. Most algorithms developed to date have focused on limiting the quasi-steady-state response of parameters such as main rotor torque, load factor, and angle of attack. For these limits, the limited parameters exhibit a proportional-type response to the pilot controls, in that they approach a quasi-steady equilibrium when a pilot applies a step input. The objective of the cueing system is to limit this quasi-steady response, while transient overshoots of the limit are allowed.

For parameters such as main rotor hub moment and main rotor flapping, the transient peak response is critical, and limiting of the quasi-steady response is not generally important. An algorithm was developed to calculate constraints on longitudinal cyclic control stick to limit the longitudinal flapping response on the XV-15 tilt rotor.[7,8] This method uses a peak response estimation algorithm based on simplified second-order linear models of the coupled vehicle/flapping dynamics. The algorithm was tested using batch simulations with prescribed control inputs (without a pilot in the loop). In the simulation testing, the stick travel was automatically constrained and was not coupled to the force-feel system. It was found that the stick constraints were highly dynamic, in that they tended to relax immediately after the initial control input, resulting in an effective rate limit. There was some concern with regard to the use of tactile cueing with highly dynamic soft stop cues because biomechanical and human factor issues might make it unfeasible.

These concerns have been addressed in a recent study on tactile cueing system designed to prevent violations of the longitudinal hub moment limit on the RAH-66 Comanche.[11] The system was tested in piloted simulation using an advanced active control stick architecture.[12] The results showed that the system was effective in helping pilots avoid hub moment limits and that the highly dynamic soft stop cues were acceptable to the pilots. The prediction algorithm used in that study differs significantly from the algorithm presented in this paper. Moreover, only longitudinal stick cues were used in the RAH-66 study. Although the longitudinal component of hub moment tends to be higher than the lateral component, the contribution from the lateral hub moment and lateral cyclic inputs should not be ignored. However, the results of this study were encouraging because it revealed that there were no fundamental biomechanical problems associated with the highly dynamic tactile cues.

The objective of the present study is to develop an algorithm that can be used to constrain simultaneously both lateral and longitudinal stick motion corresponding to a limit on the total hub moment. Note that the objective of this paper is to develop a system that helps avoid exceeding static load limits on the main rotor hub during maneuvering flight. The system does not attempt to limit or reduce vibratory hub loads associated with fatigue damage. (The same can be said for the hub load limiting system investigated for the RAH-66.[11,12]) The algorithm is designed to ensure that the peak quasi-steady hub moment, generated by lateral and longitudinal control inputs, remains within prescribed structural limits. The peak response estimation algorithm developed in Refs. 7 and 8 has been extended and is applied to limit main rotor hub moment. The main improvements are as follows: 1) The system limits total hub moment by imposing a two-dimensional constraint on lateral and longitudinal cyclic stick. 2) The prediction algorithm uses a higher-order linear model of the system dynamics. 3) The system is coupled with a model of the force-feel system dynamics and tested using a simple pilot model, which is used to replicate pilot force in cyclic stick using proportional–integral–derivative (PID) controllers. Thus, the feasibility of applying highly dynamic soft stop cues is addressed to some extent, although pilot-in-the-loop simulation will eventually be required.

Problem Motivation

Main rotor hub moment limits, also known as mast bending limits, present a difficult challenge for the development of a carefree handling control system. Limits on the maximum main rotor hub moment can be approached during highly aggressive maneuvers, when the c.g. is near operational limits, or during ground operations, when the attitude of the aircraft is constrained. In flight, hub moment is a highly dynamic parameter, and limits tend to be reached during the peak response immediately after a large control input or control reversal. After the initial control input, the magnitude of the hub moment tends to subside as the airframe responds to the applied moment. Hub moment limits are most likely to be exceeded in the longitudinal axis because of the higher moment of inertia and larger cyclic control range in the longitudinal axis. However, the total hub moment will be the vector sum of the lateral and longitudinal components, and so coupled control motions in both cyclic control axes can cause the limit to be exceeded.

Exceedence of the hub moment limit can cause deformation of the rotor mast, structural damage, reduction of component life, and possibly airframe/rotor blade interference. At the same time, main rotor hub moment is a major source of control moment in roll and pitch on a helicopter. When a very basic analysis is used, it can be shown that compliance with the Aeronautical Design Standard-33 attitude quickness requirement[13] is correlated with the maximum allowable hub moment. Suppose the pitch attitude dynamics of helicopter are represented by the following simple equations:

$$I_y \dot{q} = M, \qquad \dot{\theta} = q \tag{1}$$

In hover, the total aerodynamic moment about the c.g., M, will be dominated by the effect of the main rotor. For the UH-60A rotor system, the hub moment will represent about 60% of the total pitch moment (the other 40% coming from the tilt of the rotor thrust vector). The quickness specification requires that the pilot change aircraft attitude from the trim attitude to a new attitude as quickly as possible. The best performance can be achieved by applying maximum pitch moment over an interval of time Δt and then applying the maximum negative moment over the same interval of time to arrest the maneuver. When the interval Δt is varied, a sample of points can be calculated across the range of the quickness specification. Based on these assumptions, the peak pitch rate, the peak attitude change, and the minimum attitude change are given by

$$q_{\text{pk}} = M_{\text{lim}} \Delta t / I_y, \qquad \theta_{\text{pk}} = \theta_{\text{min}} = M_{\text{lim}} \Delta t^2 \big/ I_y \tag{2}$$

and the ratio of peak rate and peak attitude change is given by

$$q_{\text{pk}} / \theta_{\text{pk}} = 1 / \Delta t \tag{3}$$

With use of these equations and the UH-60A design moment of inertia, $I_y = 38{,}500$ ft · lb, compliance with the attitude quickness requirement can be assessed for different hub moment limits, as shown in Fig. 1. Clearly, the maximum moment achieved during the maneuver determines the performance relative to this specification.

The results discussed represent the ideal response required to achieve maximum possible performance relative to the attitude quickness specification. In reality, a pilot might have difficulty achieving this performance in flight. Other nonlinear effects, such as actuator rate and position saturation limits, will affect the results and limit performance. However, the combination of pilot and flight control system would probably not be able to achieve the maximum nose-up and nose-down pitch moment through the course of the maneuver without exceeding the static hub load limit. If the pilot must maneuver the aircraft conservatively to avoid the load limits, it may be difficult to meet the requirement. Thus, it would be desirable for the pilot to be able to approach the hub moment limit with reasonable confidence that the limit will not be exceeded.

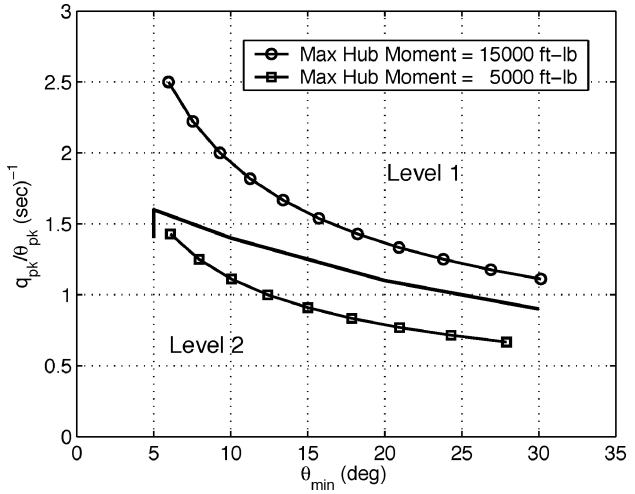

Fig. 1 Correlation of hub moment limit and attitude quickness.

There is a strong likelihood that the next generation of rotorcraft will feature carefree maneuvering systems. The inclusion of hub moment limit detection and avoidance might allow designers to reduce the structural weight in the main rotor hub. Current design standards require manufacturers to consider worst-case scenarios in establishing loads (such as a full deflection on the control sticks). Hub moment envelope protection systems could be designed to alleviate these requirements and result in less conservative structural design to save weight, while still achieving desired handling characteristics.

Theoretical Formulation

The objective of the proposed algorithm is to calculate, in real time, constraints on the cyclic stick travel that will ensure that the main rotor hub moment limit is not exceeded. These constraints can then be relayed to the pilot using a high bandwidth, programmable active control stick such as the one used in Refs. 11 and 12. The prediction algorithm monitors a number of measured flight parameters, such as angular rates in pitch and roll, the cyclic stick position, and primary servo and AFCS servoactuator positions. It uses an onboard linear model of the aircraft dynamics to estimate the combination of stick deflections that will cause the total hub moment to peak at the limit, when the current measured or estimated state of the aircraft is the initial condition.

Because the focus is on limiting the transient peak of the hub moment, the algorithm needs only to predict very near time response of the limited parameter, typically less than a second. Hence, a linear model of the fast dynamics of the rotorcraft should provide a sufficient model for prediction. Fast dynamics refers to modes with relatively high natural frequencies, or greater than about 1 rad/s for this application.

A 28-state open-loop linear model of the UH-60A operating in hover equilibrium was generated from GENHEL.[14] using a perturbation method. The model includes body dynamics, flap, lag, inflow dynamics, and engine states.

$$\begin{aligned}\boldsymbol{x} = [&u \quad v \quad w \quad p \quad q \quad r \quad \varphi \quad \theta \quad a_{0s} \quad \dot{a}_{0s} \quad \cdots\\ &a_{1s} \quad \dot{a}_{1s} \quad b_{1s} \quad \dot{b}_{1s} \quad \zeta_0 \quad \dot{\zeta}_0 \quad \zeta_{1s} \quad \dot{\zeta}_{1s} \quad \cdots\\ &\zeta_{1c} \quad \dot{\zeta}_{1c} \quad \lambda_0 \quad \lambda_{1s} \quad \lambda_{1c} \quad + 5 \text{ engine states}]^T \end{aligned} \tag{4}$$

The model was simplified by dropping states associated with the engine, heave motion, yaw motion, inflow dynamics, collective flap dynamics, and lag dynamics because these states are weakly coupled to the hub moment. Body velocities and roll and pitch angle were also dropped because they are mainly involved with the slow dynamic modes of the system. This results in a six states, reduced-order model involving roll, pitch, and lateral/longitudinal flapping. Then primary actuator models and pitch and roll Stability Augmentation System (SAS) models[14] were added to give a 13-state model. The output vector is the lateral and longitudinal component of the main rotor hub moment:

$$\begin{aligned}\boldsymbol{x} &= [p \quad q \quad a_{1s} \quad b_{1s} \quad \dot{a}_{1s} \quad \dot{b}_{1s} \quad A_{1s} \quad \dot{A}_{1s}\\ &\qquad B_{1s} \quad \dot{B}_{1s} \quad + \text{states in AFCS}]^T\\ \boldsymbol{u} &= [\delta_{\text{lat}} \quad \delta_{\text{long}}]^T\\ \boldsymbol{y} &= [L_H \quad M_H]^T = [k_{\text{hub}} b_{1s} \quad k_{\text{hub}} a_{1s}]^T\\ \Delta\dot{\boldsymbol{x}} &= \boldsymbol{A}\Delta\boldsymbol{x} + \boldsymbol{B}\Delta\boldsymbol{u}\\ \Delta\boldsymbol{y} &= \boldsymbol{C}\Delta\boldsymbol{x} \end{aligned} \tag{5}$$

Here,

$$\Delta\boldsymbol{x} = \boldsymbol{x} - \boldsymbol{x}_e, \qquad \Delta\boldsymbol{u} = \boldsymbol{u} - \boldsymbol{u}_e, \qquad \Delta\boldsymbol{y} = \boldsymbol{y} - \boldsymbol{y}_e \tag{6}$$

where e is the value in equilibrium (trimmed hover).

Figures 2 and 3 show the frequency responses of the longitudinal hub moment due to cyclic stick inputs of both the reduced-order model and the full-order nonlinear model. The data for the nonlinear model were calculated by simulating frequency sweeps in GENHEL

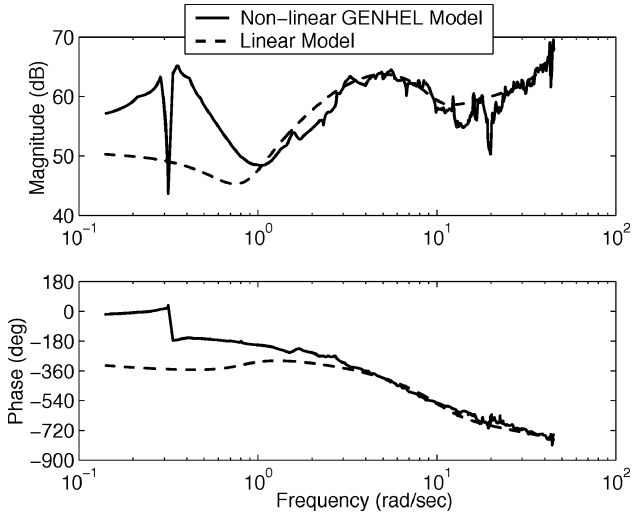

Fig. 2 Frequency response of longitudinal hub moment M_H due to lateral stick input δ_{lat}.

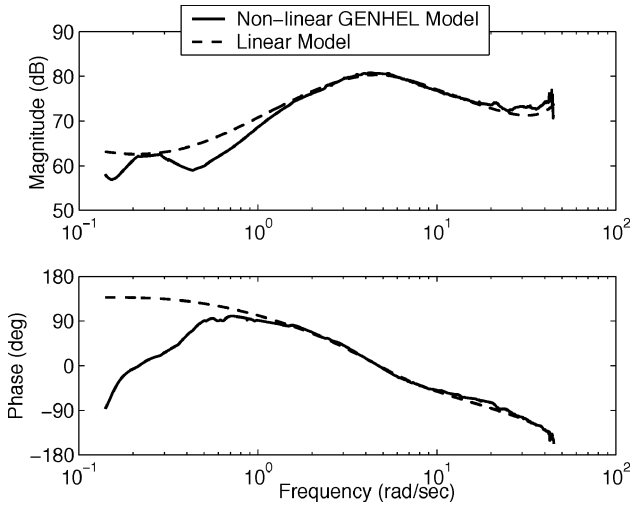

Fig. 3 Frequency response of longitudinal hub moment M_H due to longitudinal stick input δ_{long}.

and then extracting the frequency response using the software package CIFER.[15] The reduced-order model shows a good correlation with the nonlinear model at frequencies above 1 rad/s. This illustrates that the reduced-order model is a good representation of the fast dynamics. Note that it is not necessary to model dynamics at frequencies greater than the natural frequency of the flap progressive mode (about 50 rad/s). Dynamics above this frequency are critical for vibratory loads, but do not have a significant effect on the quasi-static hub loads.

Consider a step input from nonzero initial conditions, then the response of the output vector can be written as

$$\boldsymbol{y}(t) = \Delta\boldsymbol{y}(t) + \boldsymbol{y}_e = \boldsymbol{y}_e + \boldsymbol{C}e^{\boldsymbol{A}t}\Delta\boldsymbol{x}_0 + \boldsymbol{C}\boldsymbol{A}^{-1}(e^{\boldsymbol{A}t} - \boldsymbol{I})\boldsymbol{B}\Delta\boldsymbol{u} \quad (7)$$

The initial condition for the output vector can be used in place of the equilibrium value of the output,

$$\boldsymbol{y}_0 \equiv \boldsymbol{y}(0) = \boldsymbol{y}_e + \boldsymbol{C}\Delta\boldsymbol{x}_0$$

$$\Delta\boldsymbol{y}(t) = \boldsymbol{y}_0 + \boldsymbol{E}_1(t)\Delta\boldsymbol{x}_0 + \boldsymbol{E}_2(t)\Delta\boldsymbol{u} \quad (8)$$

where

$$\boldsymbol{E}_1(t) = \boldsymbol{C}(e^{\boldsymbol{A}t} - \boldsymbol{I}), \qquad \boldsymbol{E}_2(t) = \boldsymbol{C}\boldsymbol{A}^{-1}(e^{\boldsymbol{A}t} - \boldsymbol{I})\boldsymbol{B} \quad (8a)$$

The square of the quasi-static hub moment (including lateral and longitudinal components) can be written as

$$L_H^2 + M_H^2 = \|\boldsymbol{y}\|_2^2 = \Delta\boldsymbol{u}^T\boldsymbol{E}_2^T\boldsymbol{E}_2\Delta\boldsymbol{u} + 2\left(\Delta\boldsymbol{x}_0^T\boldsymbol{E}_1^T + \boldsymbol{y}_0^T\right)\boldsymbol{E}_2\Delta\boldsymbol{u}$$

$$+ \boldsymbol{y}_0^T\boldsymbol{y}_0 + 2\boldsymbol{y}_0^T\boldsymbol{E}_1\Delta\boldsymbol{x}_0 + \Delta\boldsymbol{x}_0^T\boldsymbol{E}_1^T\boldsymbol{E}_1\Delta\boldsymbol{x}_0 \quad (9)$$

or

$$L_H^2 + M_H^2 = \Delta\boldsymbol{u}^T\boldsymbol{F}\Delta\boldsymbol{u} + \boldsymbol{G}\Delta\boldsymbol{u} + H \quad (10)$$

where

$$\boldsymbol{F} = \boldsymbol{E}_2^T\boldsymbol{E}_2, \qquad \boldsymbol{G} = 2\left(\Delta\boldsymbol{x}_0^T\boldsymbol{E}_1^T + \boldsymbol{y}_0^T\right)\boldsymbol{E}_2$$

$$H = \boldsymbol{y}_0^T\boldsymbol{y}_0 + 2\boldsymbol{y}_0^T\boldsymbol{E}_1\Delta\boldsymbol{x}_0 + \Delta\boldsymbol{x}_0^T\boldsymbol{E}_1^T\boldsymbol{E}_1\Delta\boldsymbol{x}_0 \quad (10a)$$

The current values of the state vector, the stick position, and the hub moment are assumed to be known from either direct sensor measurements or a state estimator. The current states and outputs are used as the initial conditions, $\boldsymbol{x}_0$ and $\boldsymbol{y}_0$, and thus, Eq. (10) can be used to project what the magnitude of the hub moment would be at a certain time in the future. If the hub moment limit squared is put in the left-hand side of Eq. (10), then this equation describes an ellipse in the plane defined by δ_{long} and δ_{lat}. The ellipse represents a boundary on stick position within which the maximum hub moment will not be exceeded for some specified time in the future:

$$\Delta\boldsymbol{u}^T\boldsymbol{F}\Delta\boldsymbol{u} + \boldsymbol{G}\Delta\boldsymbol{u} + H = \left(L_H^2 + M_H^2\right)_{\max} \quad (11)$$

Equation (11) maps the hub moment limit into an elliptical constraint on the range of cyclic stick motion. If a set of matrices $\boldsymbol{E}_1(t)$ and $\boldsymbol{E}_2(t)$ [as defined in Eq. (8)] are calculated offline for a number of times t, then the computation of the parameters describing the elliptical stick constraint ($\boldsymbol{F}$, $\boldsymbol{G}$, and H) is relatively fast. A number of elliptical boundaries can be calculated, for various times in the future as shown in Fig. 4. The proximity of the current stick position to the elliptical boundary d can be calculated by solving the quadratic equation

$$[(\boldsymbol{n}^T\boldsymbol{F}\boldsymbol{n})/\|\boldsymbol{n}\|^2]d^2 + (\boldsymbol{G}\boldsymbol{n}/\|\boldsymbol{n}\|)d + H - \left(L_H^2 + M_H^2\right)_{\max} = 0 \quad (12)$$

where $\boldsymbol{n}$ is the gradient vector

$$\boldsymbol{n} = 2\boldsymbol{F}\Delta\boldsymbol{u}_0 + \boldsymbol{G}^T \quad (12a)$$

The boundary closest to the current stick position is chosen as the most critical constraint and is enforced using a soft stop. Thus, for some time t^*, the stick constraint will be closest to current stick position. The vector from the current stick position to the boundary is the critical control margin vector $\Delta\boldsymbol{u}^*$:

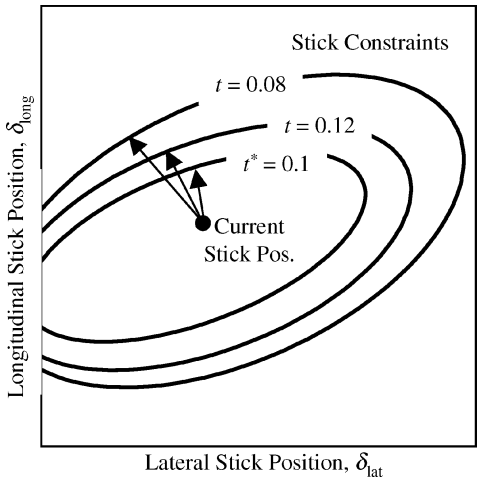

Fig. 4 Elliptical stick constraints.

$$\Delta\boldsymbol{u}^* = d^*(\boldsymbol{n}/\|\boldsymbol{n}\|) \quad (13)$$

where

$$d^* = \min_t d(t) \quad (13a)$$

The soft stop cue is imposed as the magnitude of the critical control margin drops below some threshold. In normal operation, the cyclic stick experiences a number of forces including a spring gradient, viscous damping, coulomb friction, and breakout forces. In this study, only the spring gradient and viscous damping are considered. The equations of motion for the control stick are given by

$$\begin{bmatrix} I & 0 \\ 0 & I \end{bmatrix}\ddot{\boldsymbol{u}} + \begin{bmatrix} C & 0 \\ 0 & C \end{bmatrix}\dot{\boldsymbol{u}} + \begin{bmatrix} K & 0 \\ 0 & K \end{bmatrix}\Delta\boldsymbol{u} - \boldsymbol{P}_{\text{cue}} = \boldsymbol{P} \quad (14)$$

where I, K, and C are the effective stick inertia, spring gradient, and damping coefficient, respectively, and $\boldsymbol{P}$ is the force applied by the pilot. It is assumed that there is perfect control harmony, and so the force-feel parameters are identical for the longitudinal and lateral axes and there is no coupling. The soft stop cue adds an additional term to the equations of motion for the cyclic stick:

$$\text{if } d^* > d_1 \text{ then } \boldsymbol{P}_{\text{cue}} = 0$$

$$\text{else if } d^* > d_2 \text{ then } \boldsymbol{P}_{\text{cue}} = -P_{\text{stop}}\left[\left(d^* - d_1\right)/(d_2 - d_1)\right](\boldsymbol{n}/\|\boldsymbol{n}\|)$$

$$\text{else } \boldsymbol{P}_{\text{cue}} = -P_{\text{stop}}(\boldsymbol{n}/\|\boldsymbol{n}\|) \quad (15)$$

The parameter d_1 is the threshold distance from the stick constraint where the soft stop cue is initiated, and d_2 is the distance from the constraint where the soft stop saturates. P_{stop} is the magnitude of the soft stop when it saturates. The soft stop can be more easily illustrated for a single axis, as shown in Fig. 5. In this study, the soft stop is actually implemented in two axes based on the direction of the vector $\boldsymbol{n}$. As the stick approaches the elliptical constraint, $\boldsymbol{n}$ becomes a vector normal to the constraint. The cueing force tends to push the cyclic stick in the direction that most greatly reduces the peak hub moment.

The soft stop force effectively results in an increase in spring gradient on the cyclic stick. By itself this would cause a decrease in damping ratio and, therefore, might lead to high-frequency oscillations on the stick. Therefore, a corresponding increase in damping coefficient is also applied as the soft stop is engaged to maintain a constant damping ratio.

The soft stop constraint will vary with time as the aircraft is maneuvered. If the pilot tries to push the stick beyond the constraint, the artificial force-feel system reacts with an increase in the

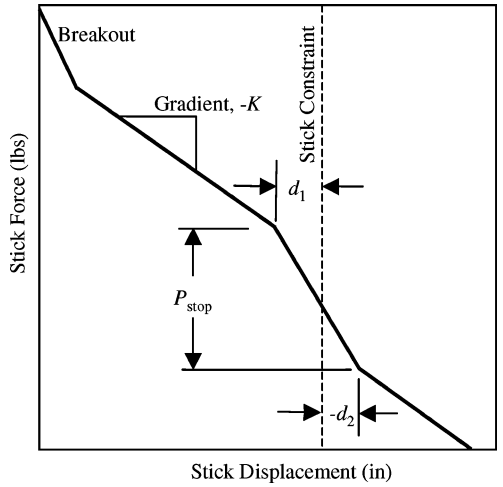

Fig. 5 Soft stop parameters (single axis).

required force to move the control stick in the direction of the constraint. The pilot can then choose to 1) backoff from the hub moment limit, 2) ride the limit to achieve maximum safe maneuverability, or 3) push through the soft stop cue and risk exceeding the hub moment limit to get even more maneuverability. This last option should be available for dire emergencies, for example, when the aircraft is approaching terrain.

Implementation and Simulation Testing

The hub moment limit detection and avoidance algorithm discussed in the preceding section was implemented in a nonlinear, blade element simulation of the UH-60A helicopter (GENHEL).[14] The algorithm was applied to limit the steady component of the total main rotor hub moment to within 15,000 ft · lb for hover and low-speed flight. This limit was chosen arbitrarily to demonstrate the algorithm and does not represent the structural load limit of the UH60A.

A linear model of the fast dynamics around the hover equilibrium [Eqs. (1–3)], was extracted from the nonlinear simulation. The resulting $\boldsymbol{A}$, $\boldsymbol{B}$, and $\boldsymbol{C}$ matrices were converted into a set of $\boldsymbol{E}_1$ and $\boldsymbol{E}_2$ matrices [Eq. (8)] for a set of horizon times ranging from 0.05 to 0.5 s with an increment of 0.01 s, and these matrices were stored for online use by the algorithm. The data storage requirements are relatively small at 15 KB. Many of the components of the state vector, such as flapping angles and rates, internal AFCS states, and servorates, would not be easily measured. Therefore, a Kalman filter state estimator was implemented. The same linear model discussed earlier was used to implement the Kalman filter. Measurements of the aircraft angular rates, primary servopositions, AFCS servopositions, and pilot stick positions were used to update the state estimate. The stick constraint calculation and the soft stop cue calculation were implemented as shown in Eqs. (11–15).

The algorithm used linear models derived about the hover trim point. In practice, it might be necessary to extract several linear models for different trim conditions and schedule them accordingly. However, it was found that the hover linear model worked well out to lateral and longitudinal speeds of 30 kn, which was adequate for this study.

The overall algorithm is somewhat computationally intensive, in that for each time step the algorithm must loop through several horizon times to find the $\boldsymbol{F}$, $\boldsymbol{G}$, and H parameters corresponding to the most critical stick constraint. The calculation is expedited by storing the $\boldsymbol{E}_1$ and $\boldsymbol{E}_2$ matrices, but note that the $\boldsymbol{G}$ and H parameters could not be stored because they are functions of the current state and control vectors. In theory the entire calculation might also be implemented as a neural network with the current state and control vectors as input. In this study, the algorithms in Eqs. (10–13) were implemented in the GENHEL simulation in FORTRAN code. The algorithm used a 10-ms update rate (the same time frame as the simulation model) and the entire simulation was able to run faster than real time on a personal computer. Thus, there is almost certainly

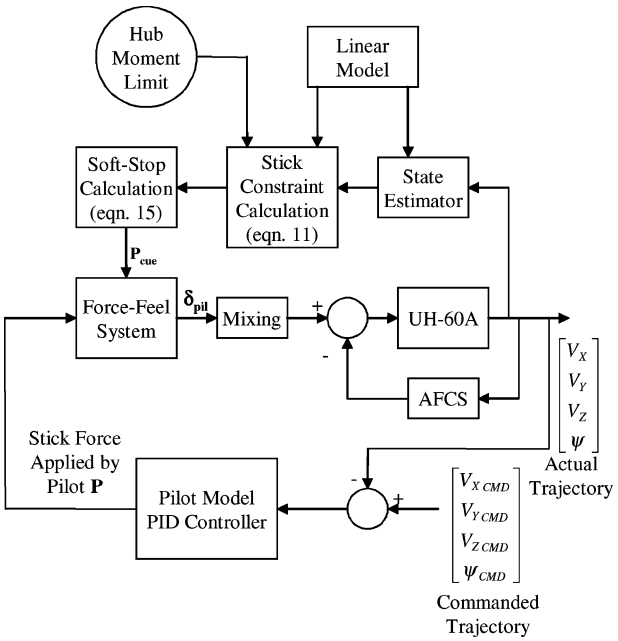

Fig. 6 Simulation model with hub moment cueing and pilot model.

available computing power on modern flight control computers to run an optimized coding of the algorithm.

In this study, the algorithm was tested in non-real-time simulation. To test the system without flight control hardware and without a pilot in the loop, a model of the force-feel system dynamics and a simple pilot model were implemented into the simulation. The force-feel system was modeled as a spring–mass–damper system [Eq. (14)] with an added term to represent the soft stop cue when the envelope cueing is engaged. In initial studies, the system was tested using prescribed force inputs, where the force vector $\boldsymbol{P}$ applied by the pilot is a prescribed function of time. In later studies, the pilot was modeled (referred as a pilot model) as a set of simple PID-type compensators, where the pilot is closing an outer loop to achieve a desired forward speed, lateral speed, vertical speed, and heading. The desired values are filtered using a first-order lag filter to achieve smooth variation:

$$\boldsymbol{P} = \begin{bmatrix} F_{\text{lat}} \\ F_{\text{long}} \end{bmatrix} = \begin{bmatrix} 0.5s + 0.5 & 0 \\ 0 & -3s - 0.5 \end{bmatrix} \begin{bmatrix} G(s)V_{y,\text{des}} - V_y \\ G(s)V_{x,\text{des}} - V_x \end{bmatrix}$$

$$\begin{bmatrix} \delta_{\text{col}} \\ \delta_{\text{ped}} \end{bmatrix} = \begin{bmatrix} 0.5 + \dfrac{0.05}{s} & 0 \\ 0 & \dfrac{2 + 20s}{0.1s + 1} \end{bmatrix} \begin{bmatrix} G(s)V_{z,\text{des}} - V_z \\ G(s)\psi_{\text{des}} - \psi \end{bmatrix} \quad (16)$$

where

$$G(s) = 1/(0.5s + 1)$$

The pilot model compensator produces an applied cyclic stick force as a feedback signal. The force is then translated into stick displacement by the force-feel system model [Eq. (14)]. Such a pilot model is required for the simulation purpose because the flight trajectory is modified dynamically as a response to the stick constraints. The overall system, as implemented in the GENHEL simulation model, is shown in Fig. 6.

Results

Initial results were obtained by simulating a maneuver where the pilot applies a diagonal force doublet on the cyclic stick. From hover, the pilot simultaneously applies a 20-lb aft and left force on the cyclic stick (ramped in over 0.5 s) and then reverses the stick by applying a 20-lb forward and right force on the stick, and then finally returning the stick to detent. The resulting aircraft velocities,

attitudes, stick positions, and hub moments are shown in Figs. 7–10, respectively. The solid lines show the results without the limit cueing system, and the dashed lines show the results with the limit cueing system. Figure 10 shows that the hub moment is greatly exceeded with no cueing. Some violations of the limit occur with the cueing, but they are relatively small. The reason is that the model used for limit prediction is linearized at hover position, whereas the algorithm was applied over a range of speeds. This drawback can be overcome by model scheduling, by calculating and storing the values of $\boldsymbol{E}_1$ and $\boldsymbol{E}_2$ for a range of airspeeds. Furthermore, a safety margin can be imposed to account for off-design conditions and to limit the required scheduling.

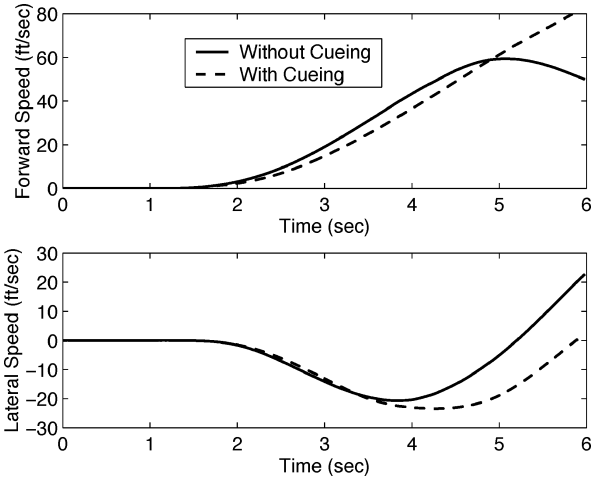

Fig. 7 Speed responses to diagonal force input.

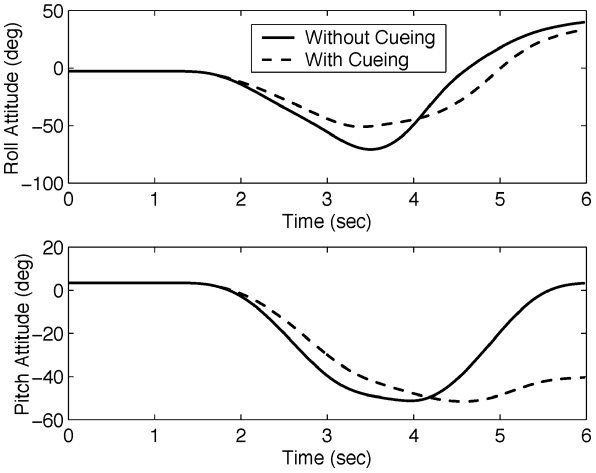

Fig. 8 Attitude responses to diagonal force input.

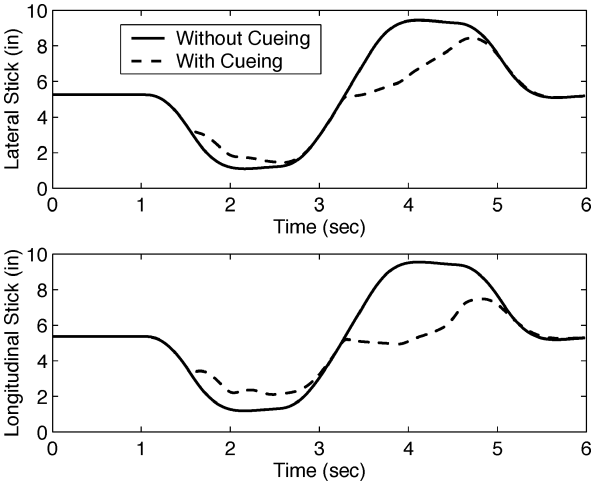

Fig. 9 Cyclic stick responses to diagonal force input.

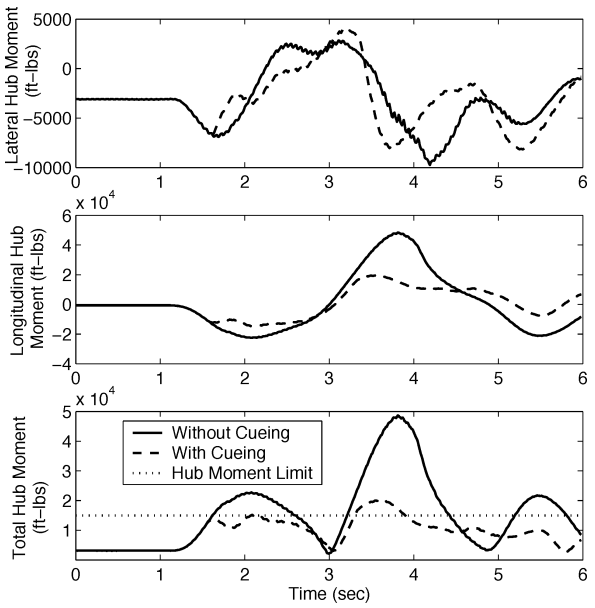

Fig. 10 Hub moment response to diagonal force input.

As shown in Fig. 9, the initial forward and left stick motion is slightly restricted when the cueing is engaged because the soft stop cue is resisting the force input, and as a result, the hub moment limit is approached but not exceeded. The purpose of showing the velocities and attitudes is to illustrate the effect of envelope limiting on the trajectory of the aircraft. The initial response of the vehicle is only slightly changed with the cueing system. As was typically observed, the most severe hub moment limits occur on control reversals. The stick travel is much more restricted, and as a result the aircraft is much slower to recover from the nose-down/left-wing-down attitude. With a real pilot in the loop, it might be expected that the pilot would continue to hold in stick pressure to recover fully from the maneuver.

The longitudinal component of the hub moment was shown to be the greatest contributor to the total hub moment because of the higher inertias and greater cyclic control range in the pitch axis. As a result, the elliptical stick constraint is tighter in the pitch axis than in the roll axis. However, the roll component makes a significant contribution, and single-axis cueing would not be effective.

The initial results using specified force inputs were useful for testing and demonstrating the basic functions of the algorithm, but it was also desired to see how the cueing would couple with the ability of the pilot to perform a task of tracking a desired trajectory. Thus, a pilot model was implemented and used to perform an aggressive acceleration/deceleration maneuver. In this maneuver, the pilot model is given longitudinal velocity commands to accelerate the aircraft from hover to 25 kn, hold for 7 s, and then decelerate back to hover again. The command is ramped in and out to achieve a 0.4 g acceleration and 0.3 g deceleration. The lateral speed, vertical speed, and heading commands are set to zero to hold lateral track and altitude.

Figures 11–14 show the resulting velocities, attitudes, stick positions, and hub moments with and without the cueing system on. As shown in Fig. 12, the resulting maneuver is very aggressive because pitch attitude excursions are greater than 30 deg in the nose-up and nose-down directions. In both cases, the commanded velocity is tracked reasonably well, although the pilot model compensator has some steady-state error. As shown in Fig. 13, the longitudinal cyclic stick is extremely active. There is a large doublet to initiate the acceleration and then arrest the acceleration to hold the target speed. There is a similar doublet for the deceleration followed by a number of oscillations to stabilize the aircraft in a hover again.

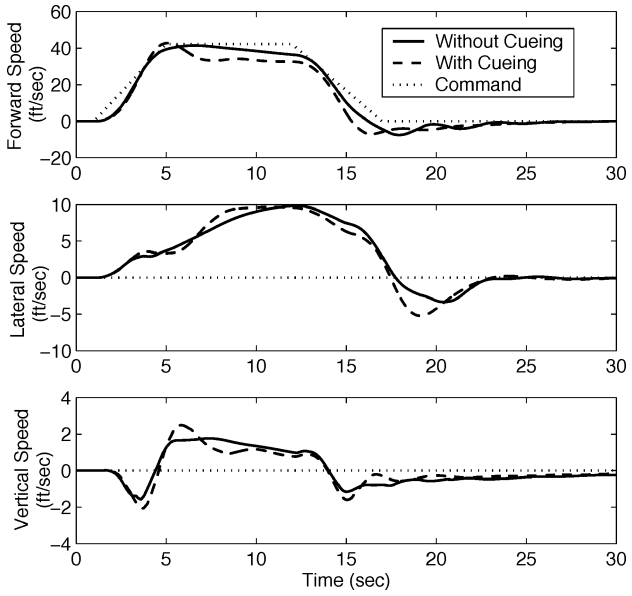

Fig. 11 Speed responses to acceleration/deceleration maneuver.

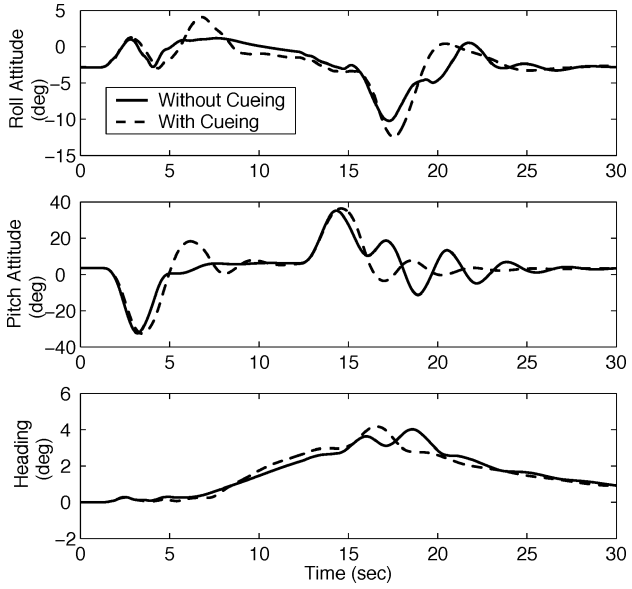

Fig. 12 Attitude responses to acceleration/deceleration maneuver.

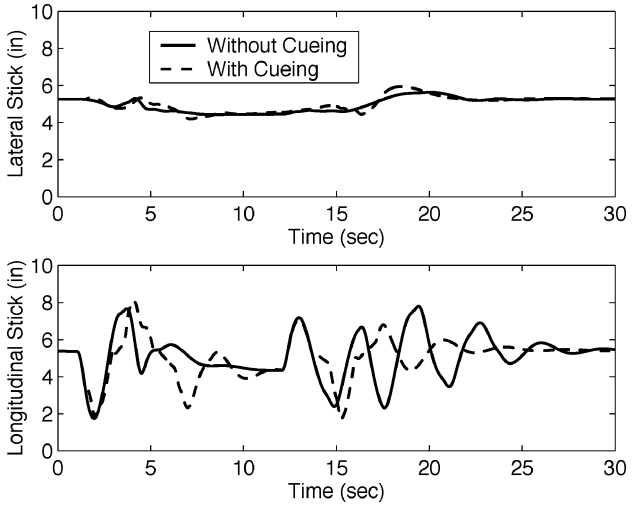

Fig. 13 Cyclic stick responses to acceleration/deceleration maneuver.

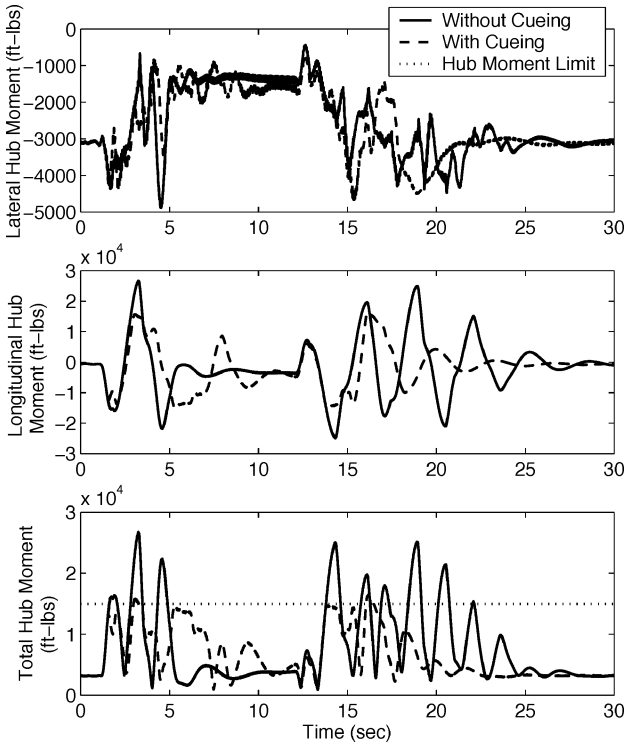

Fig. 14 Hub moment responses to acceleration/deceleration maneuver.

Figure 14 shows that the cueing performs well in keeping hub moment constrained within the prescribed limit with only a few small violations. When the pilot model attempts to track the command, there is increasing amount of force applied as the tracking error grows. Without the cueing, the stick force results in rapid motion of the stick and high hub loads. If the soft stop is engaged as the hub moment is approached, the increasing force results in a much smaller amount of stick motion, and as a result, the hub moment limit is not violated. The cost of the limiting is a slight degradation in tracking performance. This would be expected with a real pilot because the cueing effectively tells the pilot to impose rate limits and saturation limits on the control travel, which sacrifices tracking performance to stay in the envelope. The effect of cueing on stick motion is most apparent during the control reversals, for example, between 3.5 and 4.5 s, 5 and 6 s and 14 and 15 s in the longitudinal stick time history in Fig. 13. There is a rate limitlike behavior in the stick motion. During these same periods, the total hub moment in Fig. 14 is riding along the 15,000-ft · lb limit. The effective rate limit occurs because the stick constraint is dynamic and tends to relax as the pilot rides the limit.

In some cases, it was found that the pilot model could not stabilize the aircraft for very aggressive maneuvers when the limit cueing was engaged (whereas the same maneuver could be performed without the cueing). This is because, as already mentioned, the cueing results in effective rate and saturation limits, which can degrade controller performance. This is not to say that a real pilot could not stabilize the aircraft with the cueing engaged because human operators are better able to cope with nonlinearities. Real-time pilot simulation will be required to assess fully the handling qualities and biomechanical stability issues of the system.

The prediction algorithm uses a linearized model of the UH-60 dynamics at a specific operating point and for a given configuration. Inevitably, many aircraft properties such as weight and c.g. location will vary significantly during normal operation, and it would be impractical to schedule a series of linear models for all possible changes in configuration. Furthermore, there will be some uncertainty in the linear representation of the aircraft dynamics. To some extent, the results in Figs. 11–14 show that the algorithm has a certain amount of robustness, in that it operates effectively as the airspeed changes by up to 30 kn relative to the hover design point. However, a more

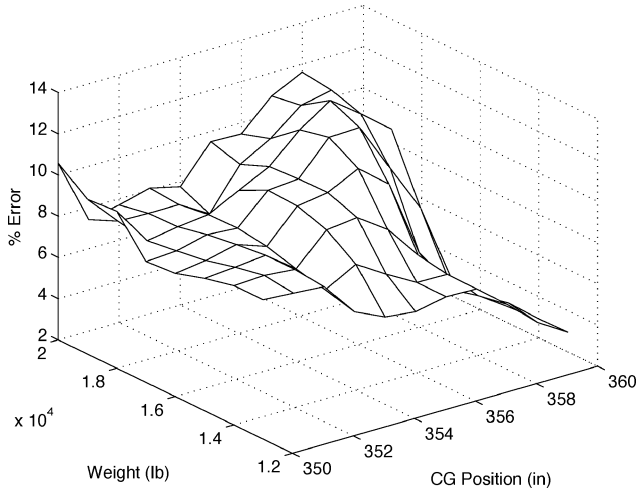

Fig. 15 Percentage error in off-design point maneuvers.

thorough investigation of off-design points is warranted. The maneuver shown in Figs. 11–14 was repeated with a number of different gross weights and longitudinal c.g. locations. The nominal weight and c.g. fuselage station are 16,825 lb and 355 in., respectively. The weight was varied from 13,000 to 20,000 lb, and the c.g. location was varied from 350 to 360 in. The desired result is that the hub moment response peak exactly at the hub moment limit when the cueing is engaged, but inevitably there are some slight overshoots of the limit. The percentage error of the system is defined as the maximum overshoot of the limit through the course of the maneuver. As long as this error is small, a safety margin could be imposed without significant loss in maneuvering performance. Figure 15 shows the percentage error for all of the combinations of weight and c.g. locations. The percentage error was within 12% for the entire range of data. This seems to indicate that an algorithm based on a single design point may have suitable robustness for implementation throughout the low-speed envelope.

Conclusions

Specific conclusions that can be drawn from the results of this research include the following:

1) According to simulation results, the hub moment limit detection and avoidance algorithm presented can provide an accurate two-dimensional constraint on cyclic stick that corresponds to the maximum peak hub moment. When the stick was held against the constraint, the hub moment was approached but rarely exceeded. In many cases, the hub moment would ride along the boundary.

2) Although the algorithm uses a linear model in the hover condition, simulation results show that it performs well when applied to a nonlinear model for speeds up to 30 kn. Furthermore, the system was tested for a range of gross weights and c.g. locations and shown to be relatively robust. Some airspeed scheduling might be required for a practical flight system to operate over the entire flight envelope.

3) Although the algorithm is computationally intensive, it can be executed in a 10-ms time frame on a personal computer at much faster than real-time speeds. Therefore, it could likely be implemented on a modern flight control computer.

4) The system was not tested with a pilot in the loop, but testing with a pilot model and force-feel system model indicated that the system is effective in reducing the likelihood of hub moment limits. The tracking performance of the pilot model, and even the ability of the pilot model to stabilize the aircraft, was sometimes sacrificed. This was because the cueing effectively imposes rate limits on the pilot control inputs. The effect on a real pilot needs to be evaluated in a real-time simulator and eventually flight tests.

It is likely that the overall effect of the system would depend greatly on the way a pilot operates an aircraft. If the pilot is typically careful not to cause excessive hub moments, then the system might alleviate this concern, the pilot could maneuver more aggressively, concentrate more on performing a task, and handling qualities might be improved. On the other hand, if the pilot does not normally care about hub moment limits, then the system would likely result in an apparent increase in workload because of the effective rate and saturation limits on the pilot's control. However, the risk of permanent structural damage would be decreased, and component life might be increased. Clearly, followon investigations of the algorithm should include real-time piloted simulation to assess 1) the feasibility of implementing the hub moment limit detection and avoidance algorithm in real time, 2) the feasibility of interfacing the algorithm with an active control stick, 3) the biomechanical stability and human factors issues associated with dynamic soft stops, and 4) the impact of the cueing on handling qualities for typical military mission tasks.

Acknowledgments

This research is being funded by the National Rotorcraft Technology Center, under the Pennsylvania State University Rotorcraft Center grant.

References

[1]Howitt, J., "Carefree Maneuvering in Helicopter Flight Control," *Proceedings of the American Helicopter Society 51st Annual Forum*, Vol. 1, American Helicopter Society, Alexandria, VA, 1995, pp. 287–298.

[2]Loy, K., "Carefree Handling and Its Applications To Military Helicopters and Missions," *Proceedings of the American Helicopter Society 53rd Annual Forum*, Vol. 1, American Helicopter Society, Alexandria, VA, 1997, pp. 489–493.

[3]Whalley, M. S., and Achache, M., "Joint U.S./France Investigation of Helicopter Flight Envelope Limit Cueing," *Proceedings of the American Helicopter Society 52nd Annual Forum*, Vol. 2, American Helicopter Society, Alexandria, VA, June 1996, pp. 1589–1617.

[4]Whalley, M. S., Hindson, W. S., and Thiers, G. G., "A Comparison of Active Sidestick and Conventional Inceptors for Helicopter Flight Envelope Tactile Cueing," *Proceedings of the American Helicopter Society 56th Annual Forum*, Vol. 1, American Helicopter Society, Alexandria, VA, 2000, pp. 181–204.

[5]Handcock, A., Lane, R., Johns, S., Howitt, J., and Charlton, M., "Benefits of Advanced Control Technology," *Proceedings of the American Helicopter Society 56th Annual Forum*, Vol. 1, American Helicopter Society, Alexandria, VA, 2000, pp. 147–156.

[6]Horn, J. F., Calise, A. C., and Prasad, J. V. R., "Flight Envelope Limiting Systems Using Neural Networks," *Proceedings of the AIAA Atmospheric Flight Mechanics Conference*, AIAA, Reston, VA, 1998, pp. 741–751.

[7]Horn, J. F., Calise, A. C., and Prasad, J. V. R., "Development of Envelope Protection Systems for Rotorcraft," *Proceedings of the American Helicopter Society 55th Annual Forum*, Vol. 2, American Helicopter Society, Alexandria, VA, 1999, pp. 2025–2036.

[8]Horn, J. F., Calise, A. C., and Prasad, J. V. R., "Flight Envelope Limit Detection and Avoidance for Rotorcraft," *Proceedings of the 25th European Rotorcraft Forum*, Vol. 2, National Aerospace Laboratory, NLR, Amsterdam, Sept. 1999.

[9]Horn, J. F., Calise, A. C., and Prasad, J. V. R., "Flight Envelope Cueing on a Tilt-Rotor Aircraft Using Neural Network Limit Prediction," *Journal of the American Helicopter Society*, Vol. 46, No. 1, 2001, pp. 23–31.

[10]Bateman, A., Ward, D., Barron, R., and Whalley, M., "A Piloted Simulation Evaluation of a Neural Network Limit Avoidance System for Rotorcraft," *Proceedings of the AIAA Atmospheric Flight Mechanics Conference*, AIAA, Reston, VA, 1999, pp. 661–673.

[11]Einthoven, P. G., "Conclusions from Active Center Stick Evaluations in the V-22 Simulator," *Proceedings of the American Helicopter Society 56th Annual Forum*, Vol. 1, American Helicopter Society, Alexandria, VA, 2000, pp. 446–457.

[12]Einthoven, P. G., Miller, D. G., Nicholas, J. S., and Margetich, S. J., "Tactile Cueing Experiments with a Three Axis Sidestick," *Proceedings of the American Helicopter Society 57th Annual Forum*, Vol. 1, American Helicopter Society, Alexandria, VA, 2001, pp. 779–794.

[13]"Handling Requirements for Military Rotorcraft," U.S. Army Aviation and Troop Command, Rept. ADS-33D-PRF, St. Louis, MO, May 1996.

[14]Howlett, J., "UH-60A BLACK HAWK Engineering Simulation Program: Volume I—Mathematical Model," NASA CR-177542, USAAVSCOM TR 89-A-001, Sept. 1989.

[15]Tischler, M. B., and Cauffman, M. G., "Frequency Response Methods for Rotorcraft System Identification: Flight Application to BO-105 Coupled Rotor/Fuselage Dynamics," *Journal of American Helicopter Society*, Vol. 37, No. 3, 1992, pp. 3–17.